Chemical Engineering Journal 156 (2010) 321–327

Contents lists available at ScienceDirect

Chemical Engineering Journal

journal homepage: www.elsevier.com/locate/cej

The low-temperature SCR of NO over rice straw and sewage sludge derived char

Jin Sun Cha[a], Jong-Cheol Choi[a], Jeong Huy Ko[a], Young-Kwon Park[a,*], Sung Hoon Park[b], Kwang-Eun Jeong[c], Seung-Soo Kim[d], Jong-Ki Jeon[e,**]

[a] Faculty of Environmental Engineering, University of Seoul, 90 Jeonnong-dong, Dongdaemun-gu, Seoul 130-743, Republic of Korea
[b] Department of Environmental Engineering, Sunchon National University, Suncheon 540-742, Republic of Korea
[c] Green Chemistry Research Division, Korea Research Institute of Chemical Technology, Daejeon 305-600, Republic of Korea
[d] Department of Chemical Engineering, Kangwon National University, Samcheok 245-711, Republic of Korea
[e] Department of Chemical Engineering, Kongju National University, Gongju 314-701, Republic of Korea

ARTICLE INFO

Article history:
Received 6 April 2009
Received in revised form 7 October 2009
Accepted 9 October 2009

Keywords:
Selective catalytic reduction (SCR)
Manganese
Chemical activation
Rice straw char
Sewage sludge char

ABSTRACT

Rice straw char and sewage sludge char were applied as catalysts for selective catalytic reduction between 50 and 250 °C using ammonia as the reducing agent. Each char was activated physically, using water vapor, or chemically, using KOH. The characteristics of the prepared catalysts were analyzed through elemental analysis, N_2 adsorption–desorption, FT-IR, NO-TPD, NH_3-TPD, and NO_x removal efficiency. The physically activated chars showed characteristics similar to those of the non-activated chars, whereas the chemically activated chars exhibited increased specific surface areas, pore volumes, NO adsorption capacities, NH_3 adsorption capacities, and oxygen functional group amounts, leading to higher NO_x removal efficiency. When the catalysts were impregnated with 3 wt% manganese, NO_x removal efficiency significantly increased. In particular, the NO_x removal efficiency was highest when the chemically activated chars were impregnated with manganese.

1. Introduction

Nitrogen oxides (NO_x) are toxic air pollutants that cause respiratory diseases in humans and animals through respiratory cell damage. They are also the primary causes of acid rain, photochemical smog, and ozone destruction [1]. Among the various measures employed to reduce NO_x emissions, selective catalytic reduction (SCR) is the most widely used worldwide. A number of investigations into catalysts for SCR processes have been undertaken [2]. The catalysts most frequently used to reduce NO_x emissions from stationary sources such as incinerators and power plants are V_2O_5/TiO_2 (anatase) catalysts mixed with WO_3 or MoO_3 [3]. Generally, V_2O_5 catalysts are resistant to SO_2, and their catalytic efficiencies are high. Nevertheless, they have the drawback of a narrow temperature window (300–400 °C). Moreover, within such a temperature range, the exhaust contains particulate matter that may cause catalyst deactivation and poisoning, as well as other pollutants such as SO_2 and As. Therefore, much attention has been paid to the development of low-temperature SCR catalysts, capable of activation under 300 °C [4–8].

Investigations of SCR using carbon (carbon-selective catalytic reduction, or CSCR) have been recently carried out, mainly by German and Japanese research groups. Carbon that is typically used for CSCR processes, such as activated carbon (AC), carbon fiber, and activated coke, show high NO_x removal efficiency at low temperatures (100–250 °C) and can be easily produced as pellets, resulting in a lower manufacturing cost compared to production in a honeycomb shape [5,6]. The activated carbon widely used in the CSCR processes is typically produced by carbonizing nut shells, wood [9], coal [10], lignin [11], coconut shells [12,13], or fruit pits [14], followed by activation with steam at high temperature. During the carbonizing process, the burning of biomass material creates numerous micropores, thus increasing the specific surface area and adsorption capacity. Heavy metal adsorption is thus possible, and the atomic bonds of the adsorbed nitrogen oxides and ammonia are weakened, allowing them to be more easily converted into nitrogen and water [15]. Low-temperature NO_x removal efficiency of these carbon catalysts can be further enhanced through a simple treatment that creates oxygen functional groups on their surface, which assisting the chemical adsorption/degradation of NO_x [16]. Activated carbon impregnated with metals like V, Cr, Cu, Fe, Mn, and Ni can also serve as an SCR catalyst with high NO_x removal efficiency [8,17]. Their large specific surface areas and metal impregnation capabilities, as well as their large numbers of surface functional groups, enable their use for physical and chemical adsorption in various applications. Carbon catalysts are also

* Corresponding author. Tel.: +82 2 2210 5623; fax: +82 2 2244 2245.
** Corresponding author. Tel.: +82 41 850 8644; fax: +82 41 858 2575.
E-mail addresses: catalica@uos.ac.kr (Y.-K. Park), jkjeon@kongju.ac.kr (J.-K. Jeon).

1385-8947/$ – see front matter © 2009 Elsevier B.V. All rights reserved.
doi:10.1016/j.cej.2009.10.027

manufactured in different forms (activated carbon, activated carbon fiber, carbon nanotube, and carbon black). With the exception of activated carbon, however, recently developed carbon materials are too expensive for use in CSCR processes.

Several efforts to produce carbon catalysts have been made recently, using a new carbon material, biomass char. Through pyrolysis or gasification, biomass can be used to produce bio-oil and bio-gas, both of which are drawing attention as renewable energy. Biomass char is the residual carbon formed during these processes that is usually disposed in landfills. As the use of biomass char is advantageous in terms of waste recycling and cost savings, many relevant investigations into it are under way [17].

In this study, carbon catalysts were produced using rice straw char (RC) and sludge char (SC), both obtained as residues from bioenergy generation processes using rice straw and sewage sludge. The chars were activated physically or chemically and impregnated with Mn, which bear a high NO_x removal efficiency at low temperatures [18]. To characterize the prepared catalysts and evaluate their NO_x removal efficiency, elemental analysis, N_2 adsorption–desorption, FT-IR, NO-TPD, and NH_3-TPD were carried out.

2. Experimental materials and method

2.1. Experimental materials

2.1.1. Raw materials

The rice straw of the most widely grown variety of rice in Korea was chosen for this study. The rice straws were cut in uniform lengths of ≤5 mm and then dried. Sewage sludge was obtained from Jungnang Sewage Treatment Plant in Seoul, Korea, where municipal wastewater is treated using the standard activated sludge method. The sludge was dried and sieved with a 150–200 mesh. To characterize the samples, approximate (moisture, combustible component, and ash), ultimate (C, H, O, N, and S), and metal component analyses were carried out for each sample. To produce the char, 5.0 g of pretreated rice straw and sewage sludge, respectively, were pyrolyzed in a reactor for 1 h, at 500 °C, under a N_2 flow of 50 mL/min.

2.1.2. Biomass char activation

The RC and SC produced in the previous step were activated physically or chemically. For physical activation, the 5.0 g chars were put into a reactor through which 50 mL/min of nitrogen gas, containing 40% water vapor, flowed. The reactor temperature was increased by 5 °C/min from room temperature to 700 °C, and then maintained for 1 h at 700 °C. The physically activated RC and SC will hereafter be referred to as "RCW" and "SCW," respectively. A KOH solution was used for the chemical activation as it had been reported to be a good activation agent [19]. The KOH and chars were mixed at a 1:1 ratio for 2 h, at 60 °C, and dried for 24 h in a 110 °C oven. Then 5.0 g of the samples, respectively, was taken from the dried chars and treated with nitrogen gas in the same way as in the physical activation. To remove the remaining K^+, the samples were washed with a 5.0 M HCl and then distilled water to remove the Cl^-. The washed samples were dried in a 110 °C oven for 24 h. The chemically activated RC and SC will hereafter be referred to as "RCK" and "SCK," respectively.

2.1.3. Mn loading

To investigate the effect of metal incorporation, the activated chars were impregnated with Mn, which had been reported to have a good low-temperature activity [18,20]. An $Mn(NO_3)_2$ solution was used as the Mn precursor and was controlled to 3 wt% loading using the incipient wetness method. The impregnated chars were then thermally treated with a 50 mL/min N_2 flow at 350 °C.

2.2. Experimental methods

2.2.1. Characterization

2.2.1.1. N_2 adsorption–desorption. The N_2 adsorption–desorption method was used to determine pore volume, pore size distribution, and specific surface area of the prepared catalysts. Prior to measurement, the catalysts were degassed for 10 h under a 200 °C vacuum atmosphere to remove other impurities therein (BEL Japan).

2.2.1.2. FT-IR. The FT-IR (Thermo Nicolet 380) analysis was performed from 4000 to 400 cm^{-1} to identify the oxygen functional groups (–COOH, –OH, –COO, and C=O) on the catalyst surface.

2.2.1.3. NO-TPD. The prepared catalysts were pretreated with N_2 gas for 1 h at 250 °C, in a quartz tubular reactor with an inner diameter of 10 mm and a height of 300 mm. Then, 0.5 g of the pretreated catalyst, respectively, was maintained in a reactor for 1 h to adsorb 500 ppm NO/N_2 at 125 °C. The amount of NO desorbed from the catalyst was then measured using a NO_x analyzer (42C, Thermo Ins.), while increasing the temperature by 5 °C/min from 125 to 550 °C.

2.2.1.4. NH_3-TPD. The acidity was examined using the NH_3-temperature-programmed desorption (TPD) method with a TPD/TPR 2900 analyzer (Micromeritics Instrument Co.). Prior to the measurements, the samples were first treated in a He stream at 400 °C and then cooled to 100 °C. The NH_3 adsorption was then carried out at 100 °C. After purging the samples in a He stream for 2 h to completely remove the physically adsorbed NH_3, the catalysts were heated to 400 °C at a heating rate of 10 °C/min. Desorbed NH_3 was detected using a thermal conductivity detector (TCD).

2.2.2. Catalytic activity

The NO_x removal efficiency was measured in a quartz tubular fixed-bed reactor with an inner diameter of 10 mm and a height of 300 mm. The inlet gas consisted of NO (1000 ppm), NH_3 (1000 ppm), O_2 (5%), and balance N_2. The flow rate was controlled using a mass flow controller (Sierra Instruments, Inc. and Hi-Tec Co.). A bypass line was installed to measure the inlet NO concentration. The NO concentrations of the inlet and outlet streams were measured using a NO_x analyzer (42C, Thermo Ins.) (Fig. 1). The *W*/*F* (catalyst weight/feed flow rate) ratio was 5.0 g min/L. The NO_x removal efficiency was calculated as follows:

$$NO_x \text{ removal efficiency} = \frac{[NO_x]_{in} - [NO_x]_{out}}{[NO_x]_{in}} \times 100$$

where $[NO_x]_{in}$ is the inlet concentration of NO_x and $[NO_x]_{out}$ is the outlet concentration of NO_x.

3. Results and discussion

3.1. Raw materials

Table 1 shows the results of the approximate (moisture, ash, and combustible component), elemental (C, H, O, N, and S), and metal component analyses of the rice straw and sewage sludge. Both the rice straw and the sewage sludge possessed low moisture and high combustible-component contents, which is favorable as these would lead to low energy consumption and a high production yield. The sewage sludge had a higher ash content compared to the rice straw, which could be ascribed to the abundant heavy metals of the soil component inflow from the grit chamber of the sewage treatment plant and the sewage itself.

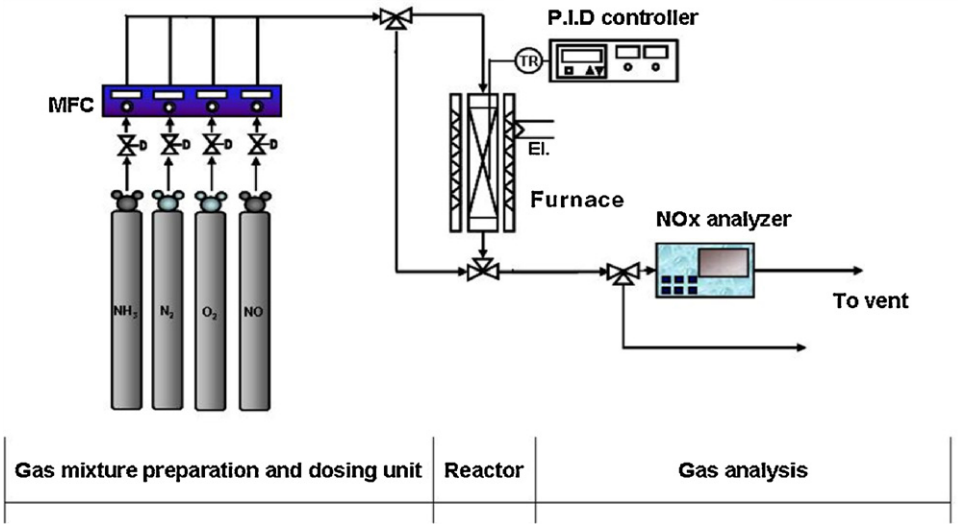

Fig. 1. Schematic diagram of experimental apparatus.

The ultimate analysis conducted in this study showed that the rice straw had a higher carbon and oxygen content compared to the sewage sludge. In particular, the oxygen content of the rice straw was more than twice that of the sewage straw, indicating that more oxygen functional groups (–COOH, –OH, –COO, and C=O) could be created from the activation of char, leading to higher catalytic activity.

The metal component analysis conducted in this study showed that the alkali metal contents (e.g., Na and K) in the rice straw were high. It is assumed that these alkali metals were absorbed from the soil together with the nutrients. The sewage sludge showed high Al, Ca, and Fe contents due to their abundance in the sewage.

3.2. Catalyst characterization

3.2.1. Rice straw char

Fig. 2 shows the N_2 adsorption–desorption isotherms of the carbon catalysts produced from RC. The isotherms show the type I shape of the BDDT classification, in which nitrogen adsorption is active at a very low p/p_0 ($p/p_0 \sim 0$), indicating micropore abundance. The adsorption capacity was shown to be higher in the order of RCK > RCW > RC, indicating that activation of the char creates more micropores and that chemical activation is more efficient in creating micropores than physical activation. In addition, the RCK showed an increase in adsorption within the ranges of mesopore and micropore, as well as in the hysteresis characteristics, which were not observed in RC and RCW, suggesting that chemical activation can also create mesopores. When the carbon catalysts were impregnated with manganese, the changes in the adsorption–desorption characteristics of MnO_x/RC and MnO_x/RCW were not large. In the case of MnO_x/RCK, the decrease in the initial adsorption compared with RCK itself suggested that the micropores were reduced by Mn impregnation.

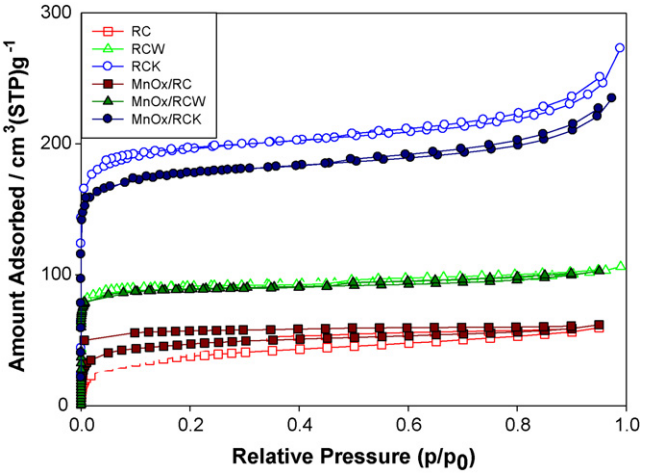

Fig. 2. Nitrogen adsorption and desorption isotherms of rice straw char based catalysts.

The specific surface area, pore volume, and pore size distribution of RC are shown in Table 2. When RC was activated (RCW and RCK),

Table 1
Physical characteristics of rice straw and sewage sludge.

Item	Unit	Rice straw	Sewage sludge
Moisture	wt%	6.8	5.56
Combustible	wt%	84.3	67.63
Ash	wt%	8.9	26.81
C	wt%	43.25	37.50
H	wt%	5.62	5.55
O	wt%	2.11	5.02
N	wt%	48.8	22.94
S	wt%	0.22	0.75
Al	ppm	295	23260
Ca	ppm	1599	19950
Cr	ppm	1460	66
Cu	ppm	562	622
Fe	ppm	5600	13090
K	ppm	9237	3498
Mg	ppm	1430	3289
Mn	ppm	2000	1208
Na	ppm	10702	5291
Ti	ppm	–	1022
Zn	ppm	80	3000

Table 2
Characterization of the rice straw char based catalysts.

Sample	BET surface area (m^2/g)	Pore volume (cm^3/g)	Ave. pore diameter (nm)
RC	139.5	0.092	2.642
RCW	363.0	0.164	1.809
RCK	772.3	0.422	2.185
MnO_x/RC	157.4	0.096	2.431
MnO_x/RCW	353.3	0.159	1.801
MnO_x/RCK	700.1	0.363	2.074

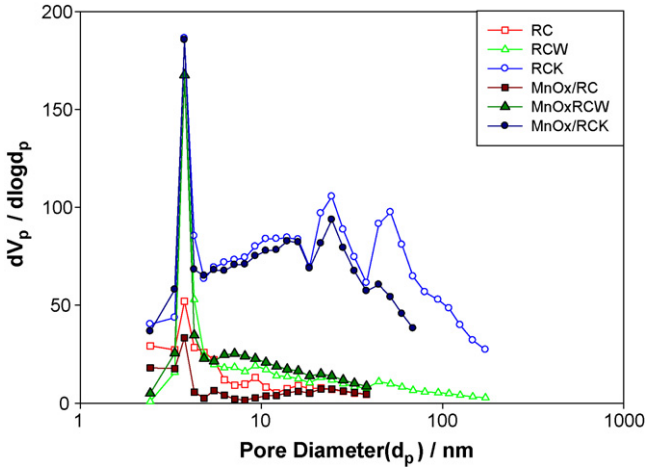

Fig. 3. BJH pore size distribution of rice straw char based catalysts.

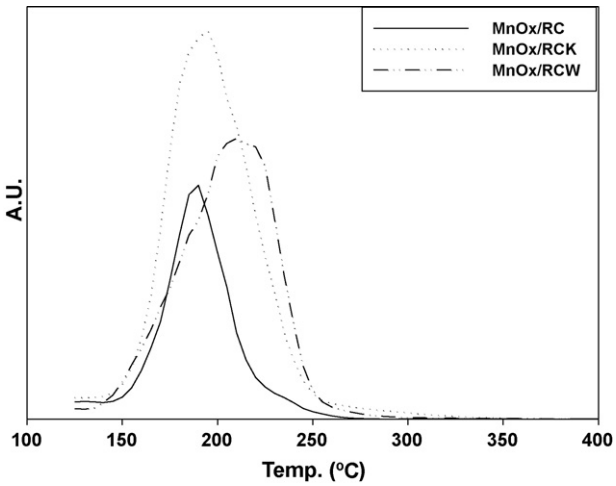

Fig. 5. NO-TPD profiles on rice char based catalysts.

its specific surface area increased considerably (139.5 m^2/g for RC, 363.0 m^2/g for RCW, and 772.3 m^2/g for RCK). Its pore volume was also considerably increased by activation. The RCK showed the highest pore volume corresponding to its highest specific surface area. The effect of Mn impregnation was different for the various substrates and the changes in specific surface area and pore volume due to Mn impregnation were not substantial.

Fig. 3 shows the pore size distribution obtained through use of the N_2 adsorption–desorption method for RC based catalysts and that the 3.7 nm pores were selectively extended, especially after activation. These pores were formed when the volatile organic matters in the samples were cracked and vaporized during pyrolysis. In the case of RCW and RCK, high-temperature activation led to formation of more pores. In particular, RCK exhibited a broad pore size distribution across larger micropore and mesopore ranges. The pore size distribution curve of Mn-impregnated RCK indicated that the number of pores was reduced during impregnation.

The FT-IR spectra of the RC based catalysts are shown in Fig. 4 for the identification of the functional groups developed on the surface. The RC, RCW, and RCK exhibited broad peaks within the range of 3500–3300 cm^{-1}, indicating the presence of hydroxyl groups therein [21–25]. The peaks that appeared at 1612 cm^{-1} appeared due to the stretching vibration of quinone and C=O [26], while the peaks at 1200 and 1110 cm^{-1} appeared due to the C–O stretching vibration [27]. The magnitudes of these peaks were in the order of RC < RCW < RCK, indicating that chemical activation of the char increased the C=O and C–O functional groups more than the other treatments.

As shown in Fig. 5, the NO-TPD was performed from 125 to 400 °C to investigate the role of chemisorbed NO. Marbán et al. [15] also performed NO-TPD from 125 to 400 °C over Mn/Activated carbon fiber. There, the authors suggested that the NO peak centered at 190 °C might correspond to desorption of the coordinated and monodentate nitrites and bridged nitrites, which can probably react with contiguously adsorbed NH_3 under SCR conditions and therefore maintain catalytic activity. As shown in Fig. 5, all of the NO-TPD peaks were centered in a range of 190–220 °C. The amounts of NO desorbed in this study were in the order of MnO_x/RCK > MnO_x/RCW > MnO_x/RC, indicating that MnO_x/RCK could produce higher amounts of active nitrites.

Fig. 6 shows that the amount of NH_3 adsorbed increased in the order of RCK > RCW ≈ RC. This seemed to be due to the high amount of oxygen functional groups and surface area of the RCK. Addition of Mn also increased the amount of NH_3 adsorbed as Mn could provide Lewis acid sites.

3.2.2. Sludge char (SC)

Fig. 7 shows the N_2 adsorption–desorption isotherms of the carbon catalysts produced from the sewage sludge char (SC). Prior to activation, the SC exhibited a non-porous type II shaped isotherm

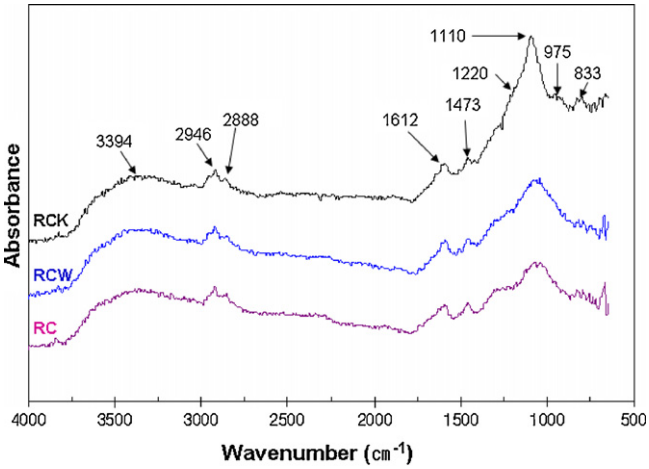

Fig. 4. FT-IR spectra of rice straw char based catalysts.

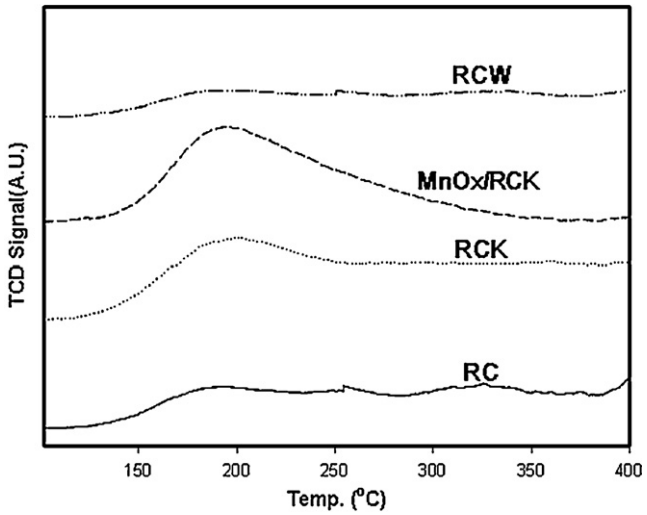

Fig. 6. NH_3-TPD profiles on rice char based catalysts.

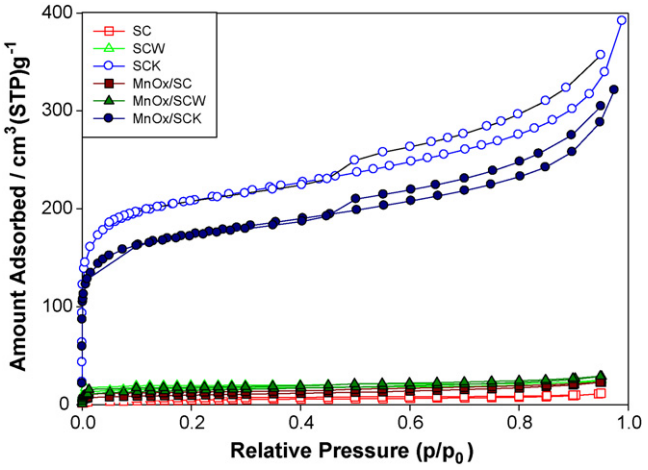

Fig. 7. Nitrogen adsorption and desorption isotherms of sludge char based catalysts.

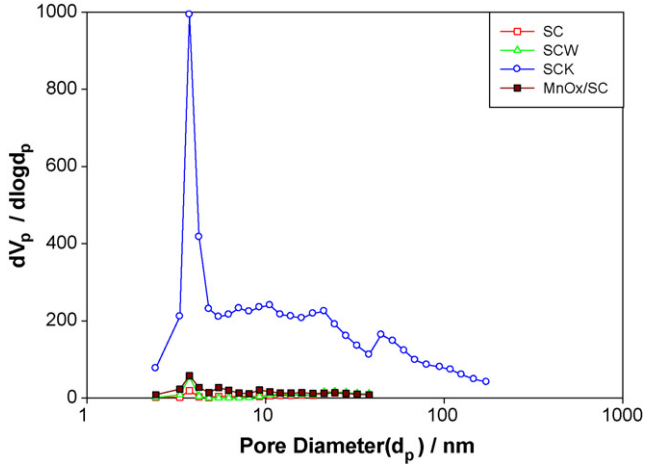

Fig. 8. BJH pore size distribution of sludge char based catalysts.

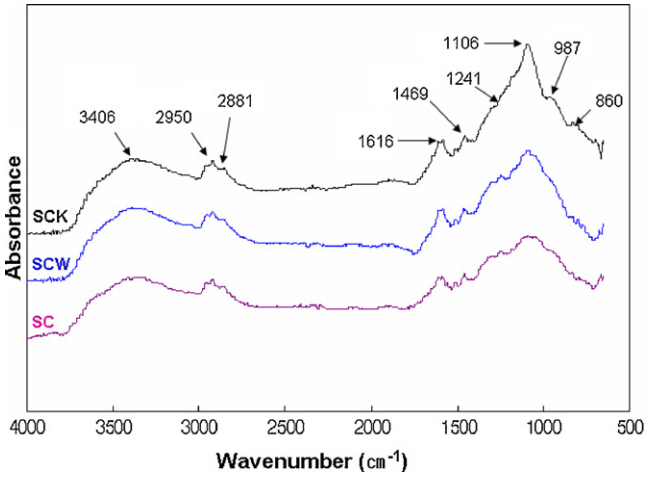

Fig. 9. FT-IR spectra of sewage sludge char based catalysts.

in which the initial adsorption was extremely low, whereas RC showed active adsorption within the micropore range (type I isotherm). This result is ascribed to the high ash and heavy metal contents of the sludge, which hinder pore formation through cracking of the organic matter during slow pyrolysis. After physical activation (SCW), the adsorption performance increased within the micropore range, but the change was lesser than that in the case of RCW. Nevertheless, adsorption performance was dramatically improved, showing a type I shaped isotherm at $p/p_0 \sim 0$, similar to the activated carbon and type IV shaped isotherm with hysteresis, within the micropore and mesopore ranges. This result can be explained as follows: the gas produced during the chemical activation is discharged quickly through the fine holes under high temperature and pressure, leaving the pores with an ink bottle shape, causing a bottleneck phenomenon during desorption after nitrogen adsorption leading to hysteresis. The Mn-impregnated-SC based catalysts showed adsorption–desorption characteristics similar to the non-impregnated, as shown in Fig. 7.

Table 3 compares the specific surface areas, pore volumes, and average pore diameters of the different kinds of SC based catalysts. Activation, especially chemical, was shown to significantly increase the specific surface areas. The specific surface areas were increased from 17.9 to 63.9 m^2/g by physical activation, and to 764.7 m^2/g by chemical activation. The order of the pore volumes was SC < SCW < SCK, corresponding to the order of the specific surface areas in the case of the RC based catalysts. Impregnation with manganese did not considerably change the characteristics shown in Table 3.

Fig. 8 shows the pore size distribution obtained through use of the N_2 adsorption–desorption method for SC based catalysts. The SC based catalysts showed pore size distributions similar to those of RC based catalysts, with the 3.7 nm pores being selectively extended, especially after activation.

Fig. 9 shows the FT-IR identification of the functional groups developed on the surface of the SC based catalysts. Generally, the SC based catalysts showed FT-IR spectra similar to those of the RC based catalysts. After chemical activation, the C=O and C–O functional groups showed the largest increase, not unlike RC.

Fig. 10 shows the NO-TPD on SC based catalysts. These catalysts showed NO-TPD similar to those of the RC based cat-

Table 3
Characterization of the sludge char based catalysts.

Sample	BET surface area (m^2/g)	Pore volume (cm^3/g)	Ave. pore diameter (nm)
SC	17.9	0.018	4.060
SCW	63.9	0.039	2.450
SCK	782.6	0.606	3.096
MnO_x/SC	35.4	0.036	4.033
MnO_x/SCW	53.8	0.045	3.348
MnO_x/SCK	645.3	0.496	3.078

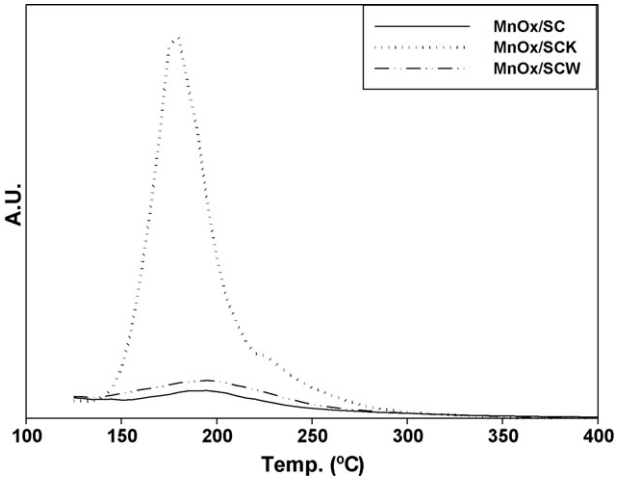

Fig. 10. NO-TPD profiles on sludge char based catalysts.

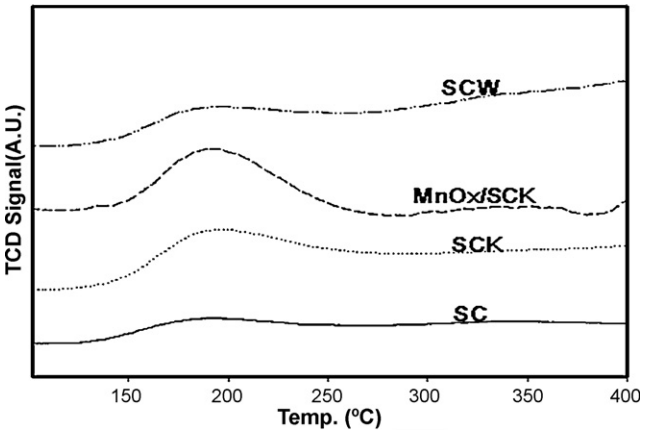

Fig. 11. NH_3-TPD profiles on sludge char based catalysts.

alysts. The amounts of NO desorbed were in the order of: MnO_x/SCK > MnO_x/SCW > MnO_x/SC.

Fig. 11 shows the NH_3-TPD of the SC based catalysts. In addition, the SC based catalysts showed NH_3-TPD similar to those of the RC based catalysts. The amounts of NH_3 adsorption were in the order of: MnO_x/SCK > SCK > SCW ≈ SC.

3.3. De-NO_x activity

3.3.1. Rice straw char (RC)

The de-NO_x performances of the RC based catalysts are shown in Fig. 12(a) as a function of temperature. At a low temperature of 50 °C, RC, RCW, and RCK exhibited 50, 71, and 86% NO_x removal efficiencies, respectively. As the temperature increased to 200 °C, respective NO_x removal efficiency was reduced to 10, 5, and 41% for RC, RCW, and RCK. At an even higher temperature of 250 °C, however, the NO_x removal efficiency increased again, making the efficiency curve V-shaped. It has been reported that in the presence of carbon catalysts, two different mechanisms may be operative in this process: adsorption of NO_x at low temperature (T < 150 °C) and reaction at higher temperature (T > 150 °C) [28]. The RCK showed the highest efficiency given its large specific surface area and abundant oxygen functional groups.

The MnO_x/RC and MnO_x/RCW, obtained by impregnating RC and RCW with manganese, showed a similar temperature dependence on de-NO_x efficiency to those of RC and RCW, as shown in Fig. 12(b). The MnO_x/RCK, however, showed significantly higher NO_x removal efficiency than the RCK at high temperatures (≥150 °C), while less than 100 °C, the NO_x removal efficiencies of MnO_x/RCK and RCK were similar. As previously stated in Section 3.2.1, the existence of highly active coordinated and monodentate nitrites and bridged nitrites produced on MnO_x/RCK can increase catalytic activity with the reacting NH_3. Additionally, increased adsorption of NH_3 on MnO_x/RCK has a high possibility of reacting with NO to result in high catalytic activity.

Furthermore, the catalytic activity of MnO_x/AC was compared with those of MnO_x/RC, MnO_x/RCW, and MnO_x/RCK catalysts. The activity of MnO_x/AC was slightly higher than that of MnO_x/RCK in a range of 150–200 °C, while the catalytic activity of MnO_x/RCK was higher than that of MnO_x/AC at a range of 50–100 °C, as well as at 250 °C. Considering the benefit of RCK as a recycled material from waste, MnO_x/RCK could be a candidate for low-temperature de-NO_x catalysts.

3.3.2. Sludge char (SC)

The de-NO_x performances of the catalysts produced from SC are shown in Fig. 13(a) as a function of temperature. At a low

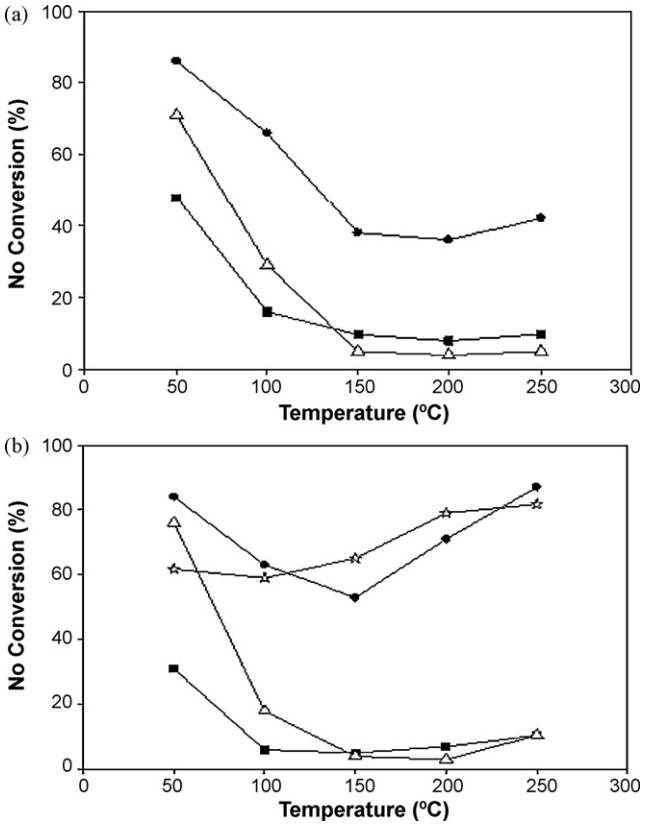

Fig. 12. NO Conversions as a function of reaction temperature: (a) RC (■), RCW (△), and RCK (●); (b) MnO_x/RC (■), MnO_x/RCW (△), MnO_x/RCK (●), and MnO_x/AC (☆).

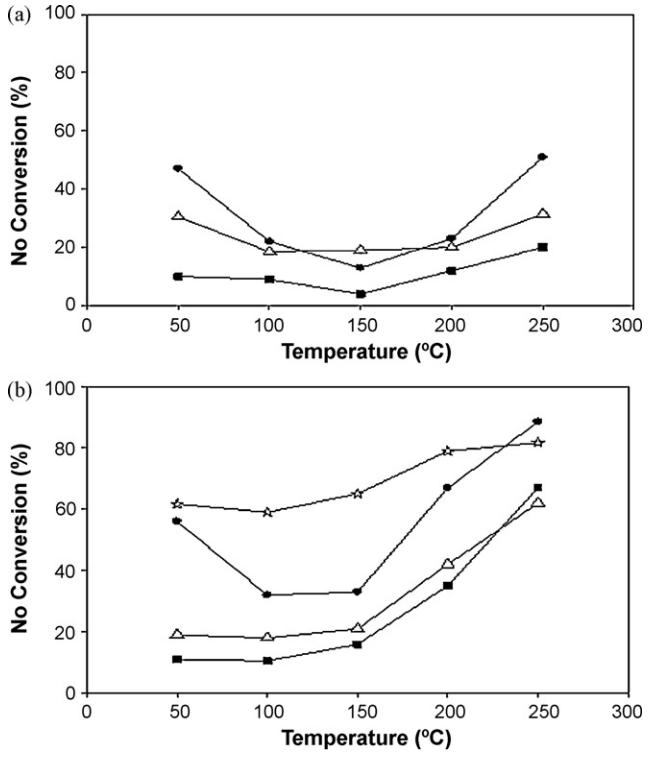

Fig. 13. NO Conversions as a function of reaction temperature: (a) SC (■), SCW (△), and SCK (●); (b) MnO_x/SC (■), MnO_x/SCW (△), MnO_x/SCK (●), and MnO_x/AC (☆).

Table 4
Metal impurities of SC and SCK.

Metal	SC (wt%)	SCK (wt%)
Al	5.9	1.6
Ca	5.1	0.4
Fe	4.8	1.9
Zn	0.3	0.1
Na	0.4	0.2
K	1.1	0.4

temperature of 50 °C, SC, SCW, and SCK exhibited 10, 30, and 46% NO_x removal efficiency, respectively. By increasing temperature to 150 °C, the NO_x reduction reaction activity was reduced to 4, 16, and 12% for SC, SCW, and SCK, respectively. At an even higher temperature of ≥200 °C, however, the NO_x removal efficiency increased again, making the efficiency curve V-shaped, as was the case for the RC based catalysts, and most likely for the same reason. The chemically activated catalyst (SCK) showed the highest efficiency due to its large specific surface area and large number of oxygen functional groups, as shown in Table 3 and Fig. 9.

The MnO_x/SC and MnO_x/SCW, obtained by impregnating SC and SCW with manganese, showed de-NO_x performances similar to those of SC and SCW at 100 °C. At temperatures over 100 °C, however, their de-NO_x efficiencies significantly increased, along with the temperature, compared to those of SC and SCW, becoming 64 and 61%, respectively, at 250 °C (Fig. 13(b)). The MnO_x/SCK showed the highest NO_x removal efficiency throughout the entire temperature range tested, which is held, as in the case of RCK, to be due to the highly active nitrites and high amounts of adsorbed NH_3 of SCK. In addition, the activity of MnO_x/SCK was similar to MnO_x/AC at 50 and 250 °C.

Although the amounts of metal impurities (e.g., K, Na, and Fe) of SCK were lower than those of SC (Table 4), the catalytic activity of SCK was higher than that of SC. This implied that the effect of metal impurities could be negligible.

4. Conclusions

Carbon catalysts were prepared using rice straw char and sewage sludge char and their NO_x removal performances evaluated. For both kinds of chars, the chemically activated catalysts exhibited higher de-NO_x efficiencies than the physically activated, which can be attributed to the larger specific surface areas, pore volumes, NO adsorption capacities, NH_3 adsorption capacities, and oxygen functional group amounts. When the catalysts were impregnated with manganese, the NO_x removal efficiencies were shown to increase throughout the entire temperature range tested. In particular, when the chemically activated chars with large specific surface areas and large numbers of oxygen functional groups were impregnated with manganese, the rice straw char exhibited 84 and 85% NO_x removal efficiency at 50 and 250 °C, respectively, and the sewage sludge char showed 55 and 85% NO_x removal efficiency at 50 and 250 °C, respectively. This study demonstrated that rice straw char and sewage sludge char could be used as raw materials of low-temperature de-NO_x carbon catalysts. Chemical activation and impregnation with transition metals such as MnO_x can be applied for even higher and more stable NO_x removal performance.

References

[1] J.C. Choi, C.H. Cho, K.E. Jeong, J.K. Jeon, J.H. Yim, Y.K. Park, Low-temperature SCR of NO over physical mixture of MnO_2 and metal-loaded activated carbon, J. Kor. Ind. Eng. Chem. 19 (2008) 92–97.
[2] F. Nakajima, I. Hamada, The state-of-the-art technology of NO_x control, Catal. Today 29 (1996) 109–115.
[3] X. Tang, J. Hao, H. Yi, J. Li, Low-temperature SCR of NO with NH_3 over AC/C supported manganese-based monolithic catalysts, Catal. Today 126 (2007) 406–411.
[4] P.A. Lowe, J.N. Armor, Low-temperature selective catalytic reduction NO_x control, ACS Symp. Series 552 (1994) 205–214.
[5] K. Kusakabe, H. Kawamura, H. Kim, S. Morooka, Effect of SO_2 on coke catalysed reduction of NO by ammonia, Fuel 69 (1990) 917–919.
[6] J. Muñiz, G. Marbán, A.B. Fuertes, Low temperature selective catalytic reduction of NO over polyarylamide-based carbon fibres, Appl. Catal. B: Environ. 23 (1999) 25–35.
[7] A. Boyano, N. Lombardo, M.E. Galvez, M.J. Lazaro, R. Moliner, Vanadium-loaded carbon-based monoliths for the on-board NO reduction: experimental study of operating conditions, Chem. Eng. J. 144 (2008) 343–351.
[8] A. Boyano, M.J. Lazaro, C. Cristiani, F.J. Maldonado-Hodar, P. Forzatti, R. Moliner, A comparative study of V_2O_5/AC and V_2O_5/Al_2O_3 catalysts for the selective catalytic reduction of NO by NH_3, Chem. Eng. J. 149 (2009) 173–182.
[9] T. Karanfil, J.E. Kilduff, Role of granular activated carbon surface chemistry on the adsorption of organic compounds. 1. Priority pollutants, Environ. Sci. Technol. 33 (1999) 3217–3224.
[10] M. Jagtoyen, M. Thwaites, J. Stencel, B. McEnaney, F. Derbyshire, Adsorbent carbon synthesis from coals by phosphoric acid activation, Carbon 30 (1992) 1089–1096.
[11] S. Johannis, S. Johannis, Activated carbon from lignocellulosic biomass-phenolic resin, J. Appl. Polym. Sci. 54 (1994) 2091–2099.
[12] J. Laine, A. Calafat, M. Labady, Preparation and characterization of activated carbons from coconut shell impregnated with phosphoric acid, Carbon 27 (1989) 191–195.
[13] J. Laine, A. Calafat, Factors affecting the preparation of activated carbons from coconut shell catalyzed by potassium, Carbon 29 (1991) 949–953.
[14] B.S. Girgis, A.N.A. El-Hendawy, Porosity development in activate carbons obtained from date pits under chemical activation with phosphoric acid, Micropor. Mesopor. Mater. 52 (2002) 105–117.
[15] G. Marbán, R. Antuña, A.B. Fuertes, Low-temperature SCR of NO_x with NH_3 over activated carbon fiber composite-supported metal oxides, Appl. Catal. B: Environ. 41 (2003) 323–338.
[16] H. Teng, Y.J. Chang, C.T. Hsieh, Performance of electric double-layer capacitors using carbons prepared from phenol–formaldehyde resins by KOH etching, Carbon 39 (2001) 1981–1987.
[17] O. Ioannidou, A. Zabaniotou, Agricultural residues as precursors for activated carbon production—a review, Renew. Sustain. Energy Rev. 11 (2007) 1966–2005.
[18] M. Yoshikawa, A. Yasutake, I. Mochida, Low-temperature selective catalytic reduction of NO_x by metal oxides supported on active carbon fibers, Appl. Catal. A: Gen. 173 (1998) 239–245.
[19] A. Ros, M.A. Lillo-Ródenas, E. Fuente, M.A. Montes-Morán, M.J. Martín, A. Linares-Solano, High surface area materials prepared from sewage sludge-based precursors, Chemosphere 65 (2006) 132–140.
[20] W.S. Kijlstra, D.S. Brands, H.I. Smit, E.K. Poels, A. Bliek, Mechanism of the selective catalytic reduction of NO with NH_3 over MnO_x/Al_2O_3, J. Catal. 171 (1997) 219–230.
[21] C. Moreno-Castilla, M.V. López-Ramón, F. Carrasco Marín, Changes in surface chemistry of activated carbons by wet oxidation, Carbon 38 (2000) 1995–2001.
[22] V. Gómez-Serrano, F. Piriz-Almeida, C.J. Durán-Valle, J. Pastor-Villegas, Formation of oxygen structures by air activation. A study by FT-IR spectroscopy, Carbon 37 (1999) 1517–1528.
[23] D.B. Mawhinney, J.T. Yates Jr., FTIR study of the oxidation of amorphous carbon by ozone at 300 K-direct COOH formation, Carbon 39 (2001) 1167–1173.
[24] B.K. Pradhan, N.K. Sandle, Effect of different oxidizing agent treatments on the surface properties of activated carbons, Carbon 37 (1999) 1323–1332.
[25] B. Buczek, S. Biniak, A. Świątkowski, Oxygen distribution within oxidised active carbon granules, Fuel 78 (1999) 1443–1448.
[26] S. Biniak, G. Szymański, J. Siedlewski, A. Świątkowski, The characterization of activated carbons with oxygen and nitrogen surface groups, Carbon 35 (1997) 1799–1810.
[27] M. Olivares-Marín, C. Fernández-González, A. Macías-García, V. Gómez-Serrano, Preparation of activated carbon from cherry stones by chemical activation with $ZnCl_2$, Appl. Surf. Sci. 252 (2006) 5967–5971.
[28] J.L. Figueiredo, M.F.R. Pereira, Carbon as catalyst, in: P. Serp, J.L. Figueiredo (Eds.), Carbon Materials for Catalysis, John Wiley & Sons, Inc., Hoboken, NJ, 2009, pp. 177–217.